Inorganic Chemistry

Article

pubs.acs.org/IC

Synthesis, Crystal Structure, and Photoelectric Properties of a New Layered Bismuth Oxysulfide

Sha Meng,[†,‡] Xian Zhang,[†,‡,§] Ganghua Zhang,[†] Yaoming Wang,[†] Hui Zhang,[†] and Fuqiang Huang*[,†,§]

[†]CAS Key Laboratory of Materials for Energy Conversion and State Key Laboratory of High Performance Ceramics and Superfine Microstructure, Shanghai Institute of Ceramics, Chinese Academy of Sciences, Shanghai 200050, People's Republic of China

[§]State Key Laboratory of Rare Earth Materials Chemistry and Applications and National Laboratory of Molecular Science, College of Chemistry and Molecular Engineering, Peking University, Beijing 100871, People's Republic of China

Supporting Information

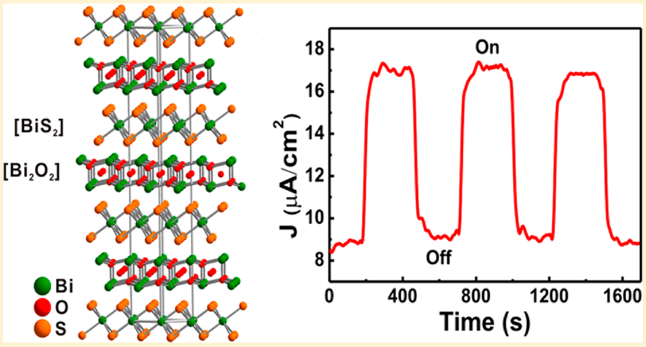

ABSTRACT: [Bi_2O_2]-containing tetragonal compounds have received enormous attention due to unique functions including ferroelectricity, photocatalysis, and superconductivity. Here, a new layered compound $Bi_9O_{7.5}S_6$ was synthesized via a facile hydrothermal route. The compound, belonging to a new structure type crystallizes in a rhombohedral system with space group $R\bar{3}m$ (a = 4.0685(1) Å, c = 31.029(5) Å, V = 444.8(1) Å^3, Z = 1). The overall crystal structure consists of alternatively packed unique [Bi_2O_2] and [BiS_2] layers along [001] which are combined with each other by van der Waals interaction. The phase purity of the product is confirmed by powder X-ray diffraction. XPS analyses indicate +3 for Bi and −2 for S atoms. The temperature dependence of resistivity $\rho(T)$ indicates that the semiconducting sample follows the mechanisms of variable range hopping (VRH) and adiabatic small polaron hopping (SPH). The direct-transition band gap, E_g = 1.27 eV derived from optical absorption spectrum, falls in the optimal region of solar absorber materials. Accordingly, the photoelectric measurement demonstrates the potential for applications for photovoltaic devices.

INTRODUCTION

Heavy p-block metals (Sn, Pb, Bi, etc.) play very important roles in multifunctional materials.[1−3] Unlike s-block metals (alkali metals, alkali earth metals) and f-block rare metals, their far-dispersed *ns* and *np* (n = 5, 6) valence orbitals are involved in constructing the valence band maximum (VBM) and conduction band minimum (CBM) near the Fermi surface in the electronic structure. Recently, Bi-containing compounds have attracted enormous attention due to their various properties. These materials include high-performance photocatalysts BiOX (X = Cl, Br, I),[4,5] layered Bi-containing ferroelectric oxides,[6] photoelectric Bi_2O_2S,[7,8] thermoelectric Bi_2O_2Se,[1,9] BiOCuS-based superconductor,[10] recently discovered superconductor $Bi_4O_4S_3$,[2,11] etc. All these materials contain the [Bi_2O_2] layers, which are two-dimensional PbO-like corner-sharing tetrahedra [OBi_4] nets. These layered structures are rather loosely packed from the packing factor model.[12] The [Bi_2O_2]-containing materials can easily form the structural/functional units, which would impact on their properties, due to the different packing habits.[13] If they have a reasonable light-driven response, they may be good photocatalysts or photovoltaic materials.[4,14]

BiOCl is a good UV-light photocatalyst, whose photocatalytic activity is superior to nanotitania (P25).[4] However, it suffers from photodecomposition under solar irradiation. Since many mixed metal oxysulfides were investigated on water splitting,[15] indicating the good chemical stability of oxysulfides. Therefore, layered bismuth oxysulfides may be fairly chemically stable and hence be more suitable for solar utilization than BiOCl and Bi_2S_3. Recently, Bi_2O_2S was demonstrated to be an excellent photoelectric material with E_g = 1.12 eV,[8] which is in the optimal band-gap region of 1.0−1.8 eV for solar absorber materials. However, Bi_2O_2S is an optically indirect-transition material which may be unable to ensure a high absorption coefficient. Therefore, in order to meet the requirements of photovoltaic materials, more layered bismuth oxysulfides need to be explored.

In this paper, a new layered bismuth oxysulfide $Bi_9O_{7.5}S_6$ has been synthesized via a facile hydrothermal route. The crystal structure belongs to a new structure type consisting of alternatively packed [Bi_2O_2] and [BiS_2]. The temperature dependence of resistivity $\rho(T)$ demonstrates that the semiconducting properties for this sample can be explained by both the variable range hopping (VRH) and the adiabatic small polaron hopping (SPH). Furthermore, the notable photoelectric responses together with the suitable direct-transition

Received: February 24, 2015
Published: May 27, 2015

DOI: 10.1021/acs.inorgchem.5b00436
Inorg. Chem. 2015, 54, 5768−5773

band gap of 1.27 eV indicate this layered bismuth oxysulfide is very promising for photovoltaic applications.

■ EXPERIMENTAL SECTION

Synthesis. The $Bi_9O_{7.5}S_6$ sample was synthesized via a reported hydrothermal method.[8] In a typical synthesis, 0.01 mol of $Bi(NO)_3$·$5H_2O$, 0.01 mol of $SC(NH_2)_2$, 5 g of KOH, and 10 g of LiOH were dissolved in a 10 mL of a mixed solution of distilled water and alcohol (volume ratio = 1:1) with continuous stirring. Then the precursors were transferred into a 50 mL Teflon-lined stainless steel autoclave to 75% of its filling capacity. The crystallization was carried out at 180 °C for 72 h. After the autoclave was cooled down to room temperature and depressurized, the product was washed with distilled water and ethanol three times and dried in an oven at 60 °C. Finally, the dark powder of single-crystal $Bi_9O_{7.5}S_6$ was obtained.

Single-Crystal and Powder X-ray Diffraction. A single crystal was analyzed by X-ray diffraction at room temperature, and data collection was performed on a Bruker D8 QUEST Diffractometer equipped with mirror-monochromated Mo Kα radiation. The structure was solved by direct methods and refined by full-matrix least-squares on F^2 using the SHELXTL program package.[16] The crystal data and refinement details are summarized in Table 1. Selected interatomic distances are presented in Table 2. The XRD patterns were characterized by an X-ray diffractometer (Bruker D8) using Cu Kα radiation (λ = 1.5418 Å) (tube voltage and electric current were 40 kV and 20 mA).

Table 1. Crystallographic Data of the Structure Refinement for $Bi_9O_{7.5}S_6$

formula	$Bi_9O_{7.5}S_6$
F_w (g·mol^{-1})	2193.18
cryst syst	trigonal
space group	$R\bar{3}m$
a (Å)	4.0685(7)
b (Å)	4.0685(7)
c (Å)	31.029(5)
α (deg)	90
β (deg)	90
γ (deg)	120
V (Å^3)	444.8(1)
cryst color	black
ρ_c (g·cm^{-3})	8.188
μ (mm^{-1})	89.397
F(000)	903
R_{int}	0.0394
R [$I > 2\sigma(I)$]	0.0220
wR_2 (all data)	0.0537
GOF	1.099

Characterization. Scanning electron microscopy (SEM) was performed on a FEI Quanta 200F microscope operating at 3 kV. Inductively coupled plasma (ICP) analysis was carried out on a PROFILE SPEC ICP instrument. The ICP analysis for the crystal sample gives rise to a concentration of Bi ions of 85.1 wt % in the compound. The oxidation states of Bi, O, and S were investigated by X-ray photoelectron spectroscopy (XPS) using an Axis Ultra spectrometer. The spectra were collected for the C 1s, Bi 4f, O 1s, and S 2s regions, and the binding energies were corrected against the C 1s reference of 284.5 eV. The ultraviolet−visible−near-infrared (UV−vis−NIR) absorption spectrum was recorded on a UV-3100 Shimadzu ultraviolet−visible−infrared spectrophotometer. The temperature variation of the resistivity, $\rho(T)$, was measured using the standard two-probe technique by the ETO model collected on the PPMS. For electric properties measurements, ceramic samples were prepared by grinding the sample powders (crystallites) and pressing them into pellets with a diameter of 5 mm under a pressure of 10 MPa. Pellets were next sealed in vacuumed quartz tubes and sintered into ceramics by firing at 500 °C for 10 h.

Table 2. Selected Interatomic Distances (Angstroms) of $Bi_9O_{7.5}S_6$

bonds		distance
Bi1−S1	×6	2.832 (3)
Bi2−O1	×1	2.16 (2)
Bi2−O1	×3	2.399 (4)
Bi2−O2	×3	2.697 (1)

Photoresponse Properties. Ceramic samples were prepared by grinding the sample powders (crystallites) and pressing them into pellets with a diameter of 5 mm under a pressure of 10 MPa. Pellets were next sealed in evacuated quartz tubes and sintered into ceramics by firing at 500 °C for 6 h. Conductivity (J−E) measurements were performed by sweeping the voltage from the positive maximum to the negative minimum using a semiconductor characterization system (KEITHLEY 4200).

Electronic Structure Calculation. The first-principles computations based on density-functional theory (DFT) were performed using the Vienna Ab-initio Simulation Package (VASP).[17] The Perdew−Burke−Ernzerhof (PBE)[18] version of the generalized gradient approximation (GGA) is used to describe the exchange correlation functional, and the projector-augmented wave (PAW)[19] method has been used in the present work. The cutoff energy of plane wave was chosen at 400 eV. For structure optimizations, 6 × 6 × 6 Monkhorst−Pack grids were used for the primitive cell and 4 × 4 × 2 k points for the conventional cell. The relaxation of geometry optimization was performed until the total energy changes within 10^{-6} eV/atom and the Hellmann−Feynman force on all atomic sites was less than 0.02 eV/Å.

■ RESULTS AND DISCUSSION

Hydrothermal synthesis at mild reaction condition is a well-defined methodology for obtaining metastable phases, which are unable to crystallize using high-temperature solid state reactions. Our newly developed hydrothermal synthesis efficiently produces nanostructured Bi_2O_2S with high phase purity in water.[8] By using alcohol as solvent and excess KOH as mineralizer, a new layered bismuth oxysulfide of $Bi_9O_{7.5}S_6$ was obtained as well-defined hexagonal plates as shown from the SEM image in Figure 1a. The EDX analysis of selected regions of the sample revealed the presence of Bi, O, and S elements (Figure S1, Supporting Information), and the average atomic ratio of Bi/S is 3:2 from different crystals. All sharp peaks in the powder XRD pattern (Figure 1b), which match the XRD pattern calculated from the crystal structure of $Bi_9O_{7.5}S_6$ (Figure S2, Supporting Information), are indexed. Figure 1c and 1d demonstrate the HRTEM image and SAED of the $Bi_9O_{7.5}S_6$ compound. Two sets of high-resolution lattice planes appear with interplanar distances of 0.321 and 0.301 nm, corresponding to (−114) and (110) atomic planes of $Bi_9O_{7.5}S_6$, respectively. The two planes also correspond to the powder XRD peaks located at 27.8° and 29.1°, respectively. The measured intersection angle between the two planes is 90°. The independent well-defined diffraction in the SAED image also declares the high degree of crystallinity. Clearly, the diffraction points of the compound have a 3-fold axis.

Single-crystal X-ray diffraction is used to determine the crystal structure of $Bi_9O_{7.5}S_6$. $Bi_9O_{7.5}S_6$ crystallizes in a rhombohedral structure with space group $R\bar{3}m$. The lattice parameters of the title compound are $a = b = 4.0685$ (1) Å and $c = 31.029$ (5) Å. The crystal structure mainly features the hexagonal layers of $[BiS_2]$ and $[Bi_2O_2]$ alternatively stacked along [001], as shown in Figure 2a. There are two unique Bi

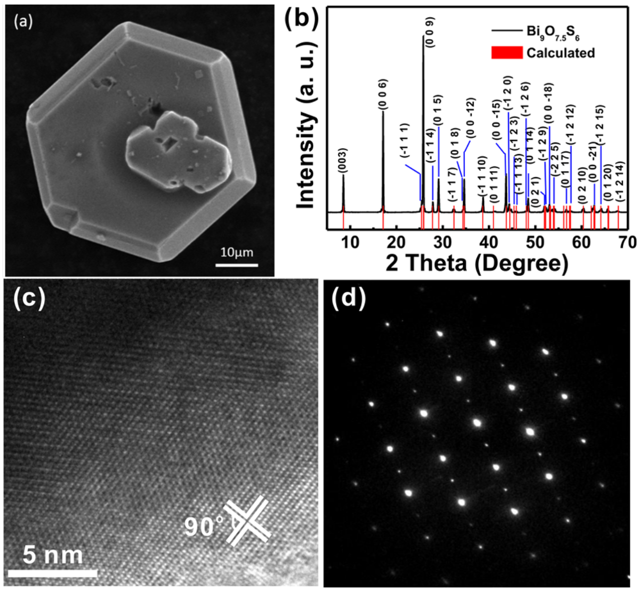

Figure 1. (a) SEM image of $Bi_9O_{7.5}S_6$ compound. (b) Powder X-ray diffraction pattern of the $Bi_9O_{7.5}S_6$ compound. (c) HRTEM image of $Bi_9O_{7.5}S_6$ compound. (d) SAED of the single crystal.

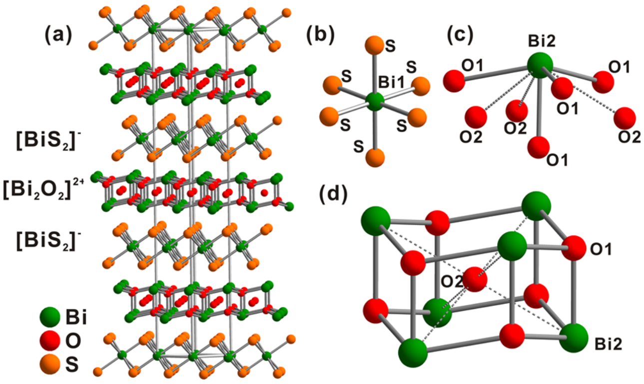

Figure 2. (a) Crystal structure of $Bi_9O_{7.5}S_6$ view done the (111) plane. Coordination environments of (b) Bi1 and (c) Bi2. (d) Hexagonal prism of $Bi2_6O1_6$ with the 50% occupancy of O2.

atoms (Bi1, Bi2), one unique S, and two unique O (O1, O2). Each Bi1 atom is coordinated to six S atoms to form a regular $[BiS_6]$ octahedron (Figure 2b). Each Bi2 is coordinated to four O1 atoms and three half-occupied O2 sites, and there is apparently a lone pair of electrons on the top of Bi2 (Figure 2c). Each O1 is tetrahedrally coordinated to four Bi2, and the S is coordinated to three Bi1 atoms with a lone pair of electrons. The half-occupied O2 site is located in the center of the distorted hexagonal prism consisting of two distorted $Bi2_3O1_3$ hexagons and coordinated to six Bi2 atoms, as shown in Figure 2d. Six Bi2 atoms in the distorted hexagonal prism form a triangular antiprism, which is also presented in the $[Al_2Si_2]$ layers of $CaAl_2Si_2$. The Bi2−O1 distance of 2.399 (4) Å is similar to that in the reported structure (2.559 in Bi_2O_3 and 2.352 Å in $Bi_4O_4S_3$).[20,21] However, the Bi2−O2 distance of 2.6974 (5) Å is longer than that of Bi2−O1. The Bi1−S distance is 2.832(3) Å, which is comparable to that in the reported structure (2.743 Å in Bi_2S_3 and 2.807 Å in $Bi_4O_4S_3$)[21,22] but shorter than that in Bi_2O_2S (3.02 Å).[23] It is worth noting that the distance of Bi2−S is about 3.26 Å, which can be attributed to van der Waals interaction.

The $[BiS_2]$ layer is a rock-salt motif of edge-sharing octahedral BiS_6 (Figure 2b), which reminds us of the hexagonal CdI_2-type (Figure 3c) transitional metal disulfide MS_2 (M = Ti, Zr, Mo),[24] which differs from the rock-salt $[BiS_2]$ layer in the superconducting $Bi_4O_4S_3$ (Figure S3, Supporting Information). The $[Bi_2O_2]$ layer is composed of an O-capped $[Bi_6]$ triangular antiprism (Figure 3a), which is present in the hexagonal phase BiO.[25] This connection is no longer the same with the tetragonal [PbO]-like $[Bi_2O_2]$ layer (Figure 3d) which is presented in other $[Bi_2O_2]$-contained compounds, for instance, BiOX, Bi_2O_2S, and $Bi_4O_4S_3$. Alternatively stacked $[BiS_2]$ and $[Bi_2O_2]$ layers are combined together by the weak Bi2···S interactions (3.26 Å), where the Bi2 atom is connected with three S and each S with three Bi2, respectively.

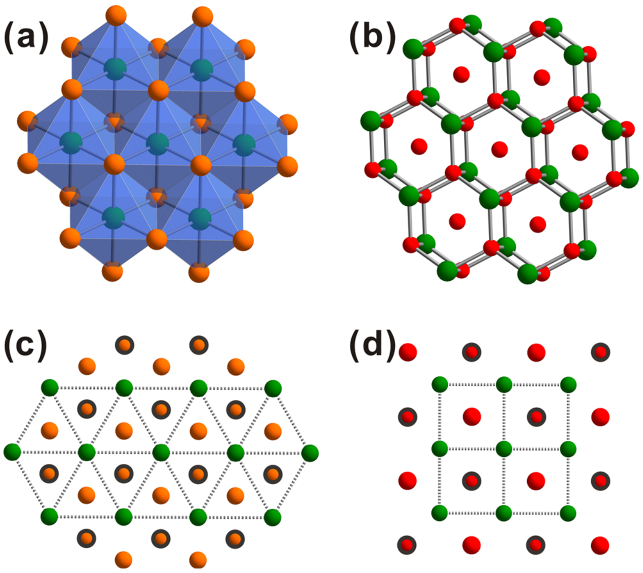

Figure 3. (a) $[BiS_2^-]$ layer viewing down the *c* axis. (b) $[Bi_2O_2^{2+}]$ layer viewing down the *c* axis. (c) Schematic hexagonal CdI_2-like sheet and (d) schematic hexagonal PbO-like sheet, where 0, *z*, and −*z* for the heights of green dots, other encircled dots, and black-circled dots, respectively.

In order to confirm the oxidation state of Bi, O, and S elements, XPS measurement was carried out for the $Bi_9O_{7.5}S_6$ compound (Figure 4). The results revealed that the binding energy of Bi $4f_{5/2}$ (164.1 eV, Figure 4a) corresponds to that of the Bi^{3+} oxidation state, and the binding energies of O 1s (531.6 eV, Figure S4b, Supporting Information) and S 2s (225.4 eV, Figure 4b) correspond to those of O^{2-} and S^{2-} oxidation states.[26] Therefore, the valence of Bi atoms is +3, whereas the O and S atoms are both −2, which is consistent with the charge

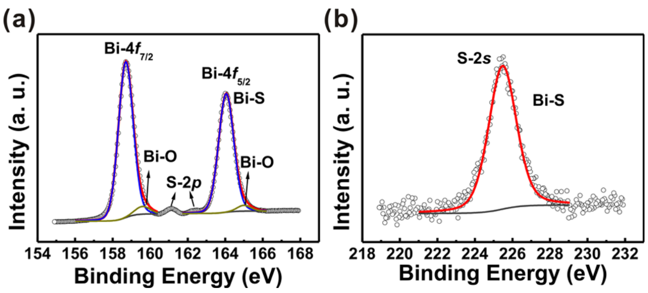

Figure 4. XPS spectra of (a) Bi $4f_{5/2}$ and (b) S 2s.

neutrality calculated for the title compound. This also explains the reason for the half occupancy of O2, which is due to charge balance.

To further confirm the semiconductor nature of the as-synthesized $Bi_9O_{7.5}S_6$ compound, we investigate the electron transport property of the compound. The temperature-dependent resistivity of the ceramic sample (calcined at 773 K) was measured from 200 to 300 K without applying a magnetic field (Figure 5). The powder XRD studies of the ceramic samples confirm the purity and homogeneity (shown in Figure S5, Supporting Information). Obviously, the resistivity of the sample exhibits a typical exponential temperature dependency, indicating a semiconducting behavior. Generally, two models were employed to describe the semiconducting transport. One is the small polaron hopping (SPH) model: $\rho(T)$ is expressed as $\rho(T)/T \propto \exp(E_P/(k_BT))$, E_p being the activation energy.[27] The other one is the variable range hopping (VRH) model: $\rho(T)$ is expressed as $\rho(T) \propto \exp(T_0/T)^{1/4}$, T_0 being the characteristic temperature.[28] For the title compound, $\rho(T)$ can be fitted using both two models, as shown in the insets in Figure 5. These phenomena were extensively observed in the other bismuth sulfides based semiconductors.[29]

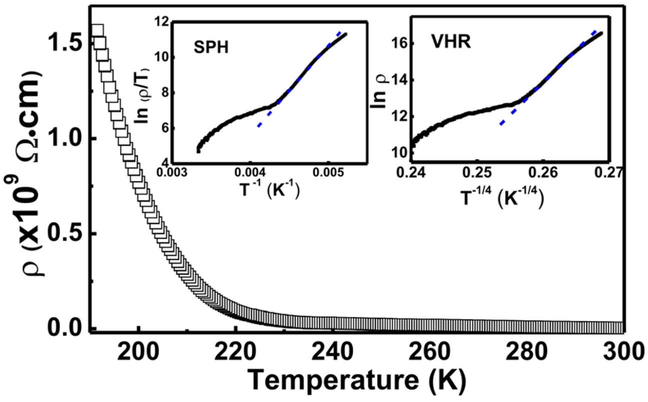

Figure 5. Temperature variation of the resistivity for $Bi_9O_{7.5}S_6$. (Insets) Plots of ln ρ vs $T^{-1/4}$ (right) and $\ln(\rho/T)$ vs $1/T$ (left). Straight lines indicate the fitting to the VRH and SPH models.

Room-temperature ultraviolet−visible−near-infrared (UV−vis−NIR) absorption spectroscopy was used to analyze the optical properties of the as-synthesized $Bi_9O_{7.5}S_6$ compound, as shown in Figure 6. The onset absorption wavelength of the gray powder is 955 nm, which is located in the infrared region, indicating a good absorption of visible light. The band gap (E_g) of $Bi_9O_{7.5}S_6$ is further explored by the extrapolation method based on Kubelka−Munk equation.[30] Figure 6 (inset) plots the $(\alpha h\nu)^2$ against the photon energy curve, where α is the absorption coefficient and $h\nu$ (h is Planck's constant, ν is the frequency) represents the photon energy. The value of E_g was estimated at 1.27 eV, which indicates that the as-synthesized $Bi_9O_{7.5}S_6$ compound is a relatively narrow band-gap semiconductor. Remarkably, the band gap is quite similar to the band gap of bulk Bi_2S_3(1.3 eV).[22] In addition, the electron transition in bulk Bi_2S_3 occurs between the Bi-6s-S-3p and the Bi-6p states. Then we can assume that the title compound may have a similar electronic structure at the valence band maximum (VBM) and conduction band minimum (CBM). Besides, the band gap is larger than that of Bi_2O_2S. As we recently found, the coplanar $[Bi_4S]$ coordination (Figure S6, Supporting Information) can reduce the coverage of Bi atoms to lead to a narrower band gap of Bi_2O_2S than that of Bi_2S_3.[8] Therefore, the more spherical coordination of the S in $Bi_9O_{7.5}S_6$, similar to that in Bi_2S_3, gives rise to a larger band gap in $Bi_9O_{7.5}S_6$ than that in Bi_2O_2S.

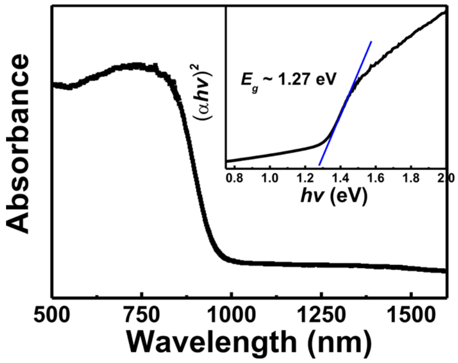

Figure 6. Ultraviolet−visible−near-infrared (UV−vis−NIR) absorption spectrum of $Bi_9O_{7.5}S_6$ sample. (Inset) Plot of $(\alpha h\nu)^2$ vs $h\nu$ for the absorption spectrum.

Considering that the band gap of the $Bi_9O_{7.5}S_6$ compound is in the range of the optimal band gap (1.3 ± 0.3 eV) for solar energy applications, the photoresponse property of the $Bi_9O_{7.5}S_6$ compound was measured. A device with sandwich structure (Figure 7a) was constructed by dropping silver paste on the $Bi_9O_{7.5}S_6$ pellet. The current−voltage ($I-V$) curve of the device is depicted in Figure 7b. Remarkable enhancement of the current density under irradiation (9 $\mu A/cm^2$ at 1 V), comparing to the dark current (4.3 $\mu A/cm^2$ at 1 V), was observed. Therefore, the $Bi_9O_{7.5}S_6$ compound has good photoelectric response properties which are attributed to the intense absorption for visible light. Two distinct states, namely, the high-current state (17 $\mu A/cm^2$ at light on) and low-current state (9 $\mu A/cm^2$ at light off), are revealed in the on/off photocurrent density plot, as shown in Figure 7c. The photocurrent is steady at both on/off states. In addition, the switch between the two states is quite sharp (Figure 7d),

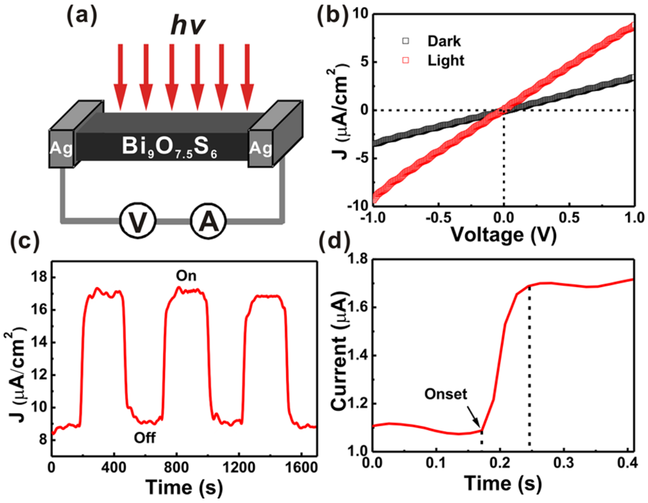

Figure 7. (a) Experimental setup of $Bi_9O_{7.5}S_6$ rectangular plate for photoresponse measurements. (b) Current−voltage curve of the as-synthesized $Bi_9O_{7.5}S_6$ tested in the dark (black) and under light (red). (c) Zero-voltage photocurrent density following on−off UV exposure. (d) Photoresponse time of the as-synthesized $Bi_9O_{7.5}S_6$.

DOI: 10.1021/acs.inorgchem.5b00436
Inorg. Chem. 2015, 54, 5768−5773

indicating the short photoresponse time (0.05 s) of the title compound. Considering the good photoresponse properties, the $Bi_9O_{7.5}S_6$ compound is a good candidate for photosensitive switch applications.

The band structure and density of states are deposited in Figure 8. The CBM and VBM are at (0, 1/2, 1/2). The band structure reveals that the $Bi_9O_{7.5}S_6$ compound has semiconductor character with a direct-transition band gap of 1.23 eV, which matches well with the UV−vis−NIR results. The partial DOS analyses indicate that the VBM consists of Bi-6s, S-3p, and O-2p states, while the CBM is mainly constructed by Bi-6p states (Figure 8c). Generally, the band gap of a material can be strongly influenced by the electronegativity difference between the cations and the anions.[31] The substitution of O for S in Bi_2S_3 increases the electronegativity difference, which should lead to the larger band gap of $Bi_9O_{7.5}S_6$ than that of Bi_2S_3. However, as mentioned above, the band gap of the $Bi_9O_{7.5}S_6$ compound is similar to that of Bi_2S_3. Such abnormal phenomenon is due to the main electron transition occuring between the Bi-6s and the Bi-6p states and the coordination of Bi atoms in $[BiS_2]^-$ layers is similar to Bi_2S_3. Therefore, the $[BiS_2]$ slabs play a very important role in the light absorption. The Bi-6s and Bi-6p states around the VBM and CBM (Figure 8a and 8c) are widely dispersed, indicating the potential high mobility for light-induced *e*−*h* separation and transport in photoelectricity. The packing factor (PF) of 0.638 is calculated from the packing factor model,[12] which is used for selecting good photocatalysts and photovoltaic materials, for instance, BiOCl (0.74), Bi_2O_2S (0.66), TiO_2 (0.65), and $KBiFeO_5$ (0.56). A lower PF structure with lower elastic stiffness provides more efficient charge separation/transport, due to the higher internal electric field, which leads to better photoelectric-related properties. In addition, atom vibrations are much easier in an open structure (lower PF value), resulting in a higher momentary polarizing field. The more polarizable structure results in larger exciton Bohr radius and hence longer carrier lifetime. The PF value around 0.65 may be critical for a good light absorber in new-concept solar cells. The title compound has a very loosely packed structure with a packing factor (PF) of 0.638, implying $Bi_9O_{7.5}S_6$ may be a good photovoltaic material.

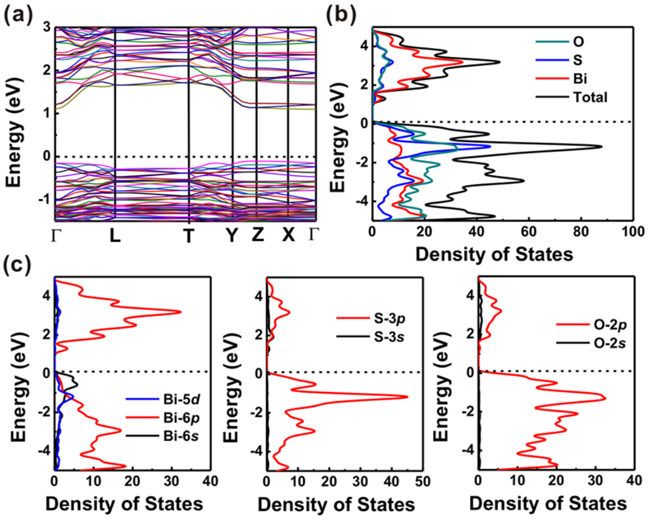

Figure 8. (a) Electronic band structure of $Bi_9O_{7.5}S_6$. (b) Total DOS of $Bi_9O_{7.5}S_6$. (c) Partial DOS of Bi, S, and O.

CONCLUSION

In summary, a new layered compound $Bi_9O_{7.5}S_6$ has been successfully synthesized via a facile hydrothermal approach. The compound, which consists of alternatively packed $[Bi_2O_2]$ and $[BiS_2]$ layers along [001], crystallizes in a rhombohedral system with space group $R\bar{3}m$. XRD confirm the phase purity of the compound, and the oxidation states of Bi (+3) and S (−2) atoms are determined by XPS. Temperature-dependent resistivity, which can be realized by both VRH and SPH models, confirms the semiconducting character of the compound. The UV−vis results show the compound has a narrow band gap of 1.27 eV, which is perfectly consistent with the first-principle calculation results. The compound was pressed into a thick film, and the film exhibits notable photoelectric behavior (light on = 9 $\mu A/cm^2$; light off = 4.3 $\mu A/cm^2$), suggesting its potential for applications for photovoltaic devices.

ASSOCIATED CONTENT

Ⓢ Supporting Information

EDS of $Bi_9O_{7.5}S_6$ single crystals; $[BiS_2]$ layer in the superconducting $Bi_4O_4S_3$; X-ray diffraction patterns for both ceramic sample and powder sample; $[BiS_2]$ layer and coplanar four-coordination of S in $Bi_9O_{7.5}S_6$. The Supporting Information is available free of charge on the ACS Publications website at DOI: 10.1021/acs.inorgchem.5b00436.

AUTHOR INFORMATION

Corresponding Author

*E-mail: huangfq@mail.sic.ac.cn.

Author Contributions

‡Sha Meng and Xian Zhang contributed equally. The manuscript was written through contributions of all authors. All authors have given approval to the final version of the manuscript.

Notes

The authors declare no competing financial interest.

ACKNOWLEDGMENTS

This work was financially supported by the Innovation Program of the CAS (Grant KJCX2-EW-W11), "Strategic Priority Research Program (B)" of the Chinese Academy of Sciences (Grants XDB04040200), NSF of China (Grants 91122034, 51125006, 61376056, 21201012, and 51402341).

REFERENCES

(1) Zhang, K.; Hu, C.; Kang, X.; Wang, S.; Xi, Y.; Liu, H. *Mater. Res. Bull.* **2013**, *48*, 3968−3972.

(2) Mizuguchi, Y.; Fujihisa, H.; Gotoh, Y.; Suzuki, K.; Usui, H.; Kuroki, K.; Demura, S.; Takano, Y.; Izawa, H.; Miura, O. *Phys. Rev. B* **2012**, *86*, 220510.

(3) (a) Zhao, L. D.; He, J. Q.; Berardan, D.; Lin, Y. H.; Li, J. F.; Nan, C. W.; Dragoe, N. *Energy Environ. Sci.* **2014**, *7*, 2900−2924. (b) Quarez, E.; Hsu, K. F.; Pcionek, R.; Frangis, N.; Polychroniadis, E. K.; Kanatzidis, M. G. *J. Am. Chem. Soc.* **2005**, *127*, 9177−9190. (c) Androulakis, J.; Lin, C. H.; Kong, H. J.; Uher, C.; Wu, C. I.; Hogan, T.; Cook, B. A.; Caillat, T.; Paraskevopoulos, K. M.; Kanatzidis, M. G. *J. Am. Chem. Soc.* **2007**, *129*, 9780−9788. (d) Tang, J.; Zou, Z.; Ye, J. *Angew. Chem., Int. Ed.* **2004**, *43*, 4463−4466. (e) Li, K.; Wang, H.; Yan, H. *J. Mol. Catal. A: Chem.* **2006**, *249*, 65−70. (f) Zhang, X.; He, J.; Chen, W.; Wang, C.; Zheng, C.; Lin, J.; Zhang, X.; Huang, F. *RSC Adv.* **2014**, *4*, 34288−34293.

(4) Zhang, K.-L.; Liu, C. M.; Huang, F. Q.; Zheng, C.; Wang, W. D. *Appl. Catal., B* **2006**, *68*, 125−129.

(5) (a) Shang, M.; Wang, W.; Zhang, L. *J. Hazard. Mater.* **2009**, *167*, 803−809. (b) Xiao, X.; Zhang, W. D. *J. Mater. Chem.* **2010**, *20*, 5866−5870.

(6) Murata, W.; Onodera, A.; Yoshio, K.; Yamashita, H.; Takama, T. *Ferroelectrics* **2002**, *270*, 303−308.

(7) Pacquette, A. L.; Hagiwara, H.; Ishihara, T.; Gewirth, A. A. *J. Photochem. Photobiol., A* **2014**, *277*, 27−36.

(8) Zhang, X.; Liu, Y.; Zhang, G.; Wang, Y.; Zhang, H.; Huang, F. *ACS Appl. Mater. Interfaces* **2015**, *7*, 4442−4448.

(9) Ruleova, P.; Drasar, C.; Lostak, P.; Li, C. P.; Ballikaya, S.; Uher, C. *Mater. Chem. Phys.* **2010**, *119*, 299−302.

(10) (a) Shein, I.; Ivanovskii, A. *Solid State Commun.* **2010**, *150*, 640−643. (b) Mazin, I. *Phys. Rev. B* **2010**, *81*, 140508. (c) Ubaldini, A.; Giannini, E.; Senatore, C.; Van Der Marel, D. *Phys. C* **2010**, *470*, S356−S357.

(11) (a) I. Sathish, C.; Luke Feng, H.; Shi, Y.; Yamaura, K. *J. Phys. Soc. Jpn.* **2013**, *82*, 074703. (b) Phelan, W. A.; Wallace, D. C.; Arpino, K. E.; Neilson, J. R.; Livi, K. J.; Seabourne, C. R.; Scott, A. J.; McQueen, T. M. *J. Am. Chem. Soc.* **2013**, *135*, 5372−5374.

(12) (a) Wu, J. J.; Li, J. T.; Lu, X. J.; Zhang, L. L.; Yao, J. Y.; Zhang, F. X.; Huang, F. Q.; Xu, F. F. *J. Mater. Chem.* **2010**, *20*, 1942−1946. (b) Wu, J.; Huang, F.; Lü, X.; Chen, P.; Wan, D.; Xu, F. *J. Mater. Chem.* **2011**, *21*, 3872−3876. (c) Wu, J.; Huang, F.; Shan, Z.; Wang, Y. *Dalton Trans.* **2011**, *40*, 6906−6911. (d) Yin, X.; Shi, L.; Wei, A.; Wan, D.; Wang, Y.; Huang, F. *J. Solid State Chem.* **2012**, *192*, 182−185. (e) Lü, X.; Yang, W.; Quan, Z.; Lin, T.; Bai, L.; Wang, L.; Huang, F.; Zhao, Y. . *Am. Chem. Soc.* **2013**, *136*, 419−426.

(13) (a) Zhang, X.; He, J. Q.; Chen, W.; Zhang, K. T.; Zheng, C.; Sun, J. L.; Liao, F. H.; Lin, J. H.; Huang, F. Q. *Chem.—Eur. J.* **2014**, *20*, 5977−5982. (b) Zhang, X.; Chen, W.; Mei, D. J.; Zheng, C.; Liao, F. H.; Li, Y. T.; Lin, J. H.; Huang, F. Q. *J. Alloys Compd.* **2014**, *610*, 671−675.

(14) Lin, X.; Wu, J.; Lü, X.; Shan, Z.; Wang, W.; Huang, F. *Phys. Chem. Chem. Phys.* **2009**, *11*, 10047−10052.

(15) (a) Ogisu, K.; Ishikawa, A.; Teramura, K.; Toda, K.; Hara, M.; Domen, K. *Chem. Lett.* **2007**, *36*, 854−855. (b) Ogisu, K.; Ishikawa, A.; Shimodaira, Y.; Takata, T.; Kobayashi, H.; Domen, K. *J. Phys. Chem. C* **2008**, *112*, 11978−11984. (c) Ishikawa, A.; Yamada, Y.; Takata, T.; Kondo, J. N.; Hara, M.; Kobayashi, H.; Domen, K. *Chem. Mater.* **2003**, *15*, 4442−4446.

(16) Farrugia, L. J. *J. Appl. Crystallogr.* **1999**, *32*, 837−838.

(17) Kresse, G.; Furthmüller, J. *Phys. Rev. B* **1996**, *54*, 11169.

(18) Perdew, J. P.; Burke, K.; Ernzerhof, M. *Phys. Rev. Lett.* **1996**, *77*, 3865.

(19) Blöchl, P. E. *Phys. Rev. B* **1994**, *50*, 17953.

(20) Hameed, A.; Montini, T.; Gombac, V.; Fornasiero, P. *J. Am. Chem. Soc.* **2008**, *130*, 9658−9659.

(21) Singh, S. K.; Kumar, A.; Gahtori, B.; Sharma, G.; Patnaik, S.; Awana, V. P. *J. Am. Chem. Soc.* **2012**, *134*, 16504−16507.

(22) Sirimanne, P. M.; Takahashi, K.; Sonoyama, N.; Sakata, T. *Sol. Energy Mater. Sol. Cells* **2002**, *73*, 175−187.

(23) Koyama, E.; Nakai, I.; Nagashima, K. *Acta Crystallogr., Sect. B: Struct. Sci.* **1984**, *40*, 105−109.

(24) (a) Yu, Y. G. G.; Ross, N. L. *J. Phys.: Condens. Matter* **2011**, *23*, 11. (b) Hagg, G.; Schonberg, N. *Ark. Kemi* **1954**, *7*, 371−380. (c) Bell, R. E.; Herfert, R. E. *J. Am. Chem. Soc.* **1957**, *79*, 3351−3354.

(25) Zavyalov, Aa; Imamov, R. M.; Pinsker, Z. G. *Sov. Phys. Cryst.* **1966**, *10*, 401−&.

(26) (a) Chen, R.; Shen, Z. R.; Wang, H.; Zhou, H.-J.; Liu, Y.-P.; Ding, D. T.; Chen, T. H. *J. Alloys Compd.* **2011**, *509*, 2588−2596. (b) Li, R.; Chen, W.; Kobayashi, H.; Ma, C. *Green Chem.* **2010**, *12*, 212−215. (c) Berglund, S. P.; Rettie, A. J.; Hoang, S.; Mullins, C. B. *Phys. Chem. Chem. Phys.* **2012**, *14*, 7065−7075.

(27) Mott, N.; Davis, E. *Electrical processes in non-crystalline materials*; Clarendon: Oxford, 1971; p 152.

(28) Mott, N. *J. Non-Cryst. Solids* **1968**, *1*, 1−17.

(29) Muntyanu, F.; Gilewski, A.; Nenkov, K.; Warchulska, J.; Zaleski, A. *Phys. Rev. B* **2006**, *73*, 132507.

(30) Kubelka, P. *Z. Technol. Phys.* **1931**, *12*, 330.

(31) Goodenough, J. B. *J. Phys. Chem. Solids* **1969**, *30*, 261−280.